JOURNAL OF MAGNETIC RESONANCE IMAGING 20:540–554 (2004)

Invited Review

Functional MRI of the Lung Using Hyperpolarized 3-Helium Gas

Edwin J.R. van Beek, MD,[1]* Jim M. Wild, PhD,[1] Hans-Ulrich Kauczor, MD,[2] Wolfgang Schreiber, PhD,[3] John P. Mugler III, PhD,[4] and Eduard E. de Lange, MD[4]

Lung imaging has traditionally relied on x-ray methods, since proton MRI is limited to some extent by low proton density in the lung parenchyma and static field inhomogeneities in the chest. The relatively recent introduction of MRI of hyperpolarized noble gases has led to a rapidly evolving field of pulmonary MRI, revealing functional information of the lungs, which were hitherto unattainable. This review article briefly describes the physical background of the technology, and subsequently focuses on its clinical applications. Four different techniques that have been used in various human investigations are discussed: ventilation distribution, ventilation dynamics, and small airway evaluation using diffusion imaging and oxygen uptake assessment.

Key Words: lung diseases; pulmonary function; hyperpolarized helium-3; MRI; ultrafast imaging
J. Magn. Reson. Imaging 2004;20:540–554.

THE DEVELOPMENT OF MR imaging of the lungs has come late compared to other regions of the body. This is largely explained by the adverse physical conditions, namely low proton density and field inhomogeneity, in the lungs. Conventional proton MRI has provided some limited anatomical information at the field strengths that are used for routine clinical imaging. However, since the introduction of hyperpolarized (HP) noble gases, such as 3-helium (3-He) and xenon-129 (129-Xe), in the 1990s, the development of functional lung MRI has taken flight through the collaborative efforts of multidisciplinary groups of scientists and clinicians. The use of these gases has paved the way for pulmonary assessment using MRI, and has resulted in novel physiological measurements that were not previously feasible with any other technique.

Until the present day, CT has been the main diagnostic modality for the evaluation of lung diseases. However, this technology is largely static, giving morphological information of high spatial resolution (in the range of 1 mm^3). Although some attempts have been made to introduce dynamic CT imaging for ventilation assessment, both with the use of standard multidetector CT and with xenon-enhanced electron beam CT, these techniques have not been introduced into clinical practice due to technical constraints and due to ionizing radiation issues (1–5). An alternative technology, ventilation scintigraphy, lacks both spatial and temporal resolution and also requires (small doses) of ionizing radiation (6–8). Thus, it is apparent that the use of MR imaging for lung assessment has great potential. First, the lack of ionizing radiation renders it the preferred technique for young patients as well as for those who require regular follow-up imaging and for tests on healthy volunteers. Second, MR imaging offers the potential of ultrafast sequences, which allow assessment of the lungs during the ventilatory cycle. Finally, the particular physical properties of hyperpolarized noble gases make it feasible to use their signal changes to extract novel data on gas exchange and lung physiology.

Lung imaging using MRI is taking shape, not only using perfusion and angiographic techniques (9), but also using hyperpolarized noble gases (Fig. 1). Since the physical background of hyperpolarized-gas imaging was reviewed recently (10), this review focuses on clinical applications and the role of hyperpolarized 3-He MR imaging compared to other novel imaging techniques. In particular, we will discuss its potential for assessing pulmonary ventilation, microstructural changes, and gas exchange.

HYPERPOLARIZED NOBLE GASES

3-He and 129-Xe have a nuclear spin of 1/2, which renders them sensitive to nuclear magnetic resonance techniques. In thermal equilibrium, the population of

[1]Academic Unit of Radiology, University of Sheffield, Sheffield, UK.
[2]German Cancer Research Center, Heidelberg, Germany.
[3]Department of Radiology, University of Mainz, Mainz, Germany.
[4]Department of Radiology, University of Virginia, Charlottesville, Virginia.

Contract grant sponsor: European Framework 5 Programme (Polarized Helium Imaging of the Lung); Contract grant sponsor: German Research Council; Contract grant number: FOR 474. Contract grant sponsor: National Institutes of Health; Contract grant number: 1R01HL6649.

*Address reprint requests to: E.J.R.V., MD, PhD, FRCR, Professor of Radiology, Carver College of Medicine, University of Iowa Hospitals and Clinics, 3895 JPP, 200 Hawkins Drive, Iowas City, IA 52242-1077. E-mail: edwin-vanbeek@uiowa.edu.

Received March 1, 2004; Accepted May 12, 2004.
DOI 10.1002/jmri.20154
Published online in Wiley InterScience (www.interscience.wiley.com).

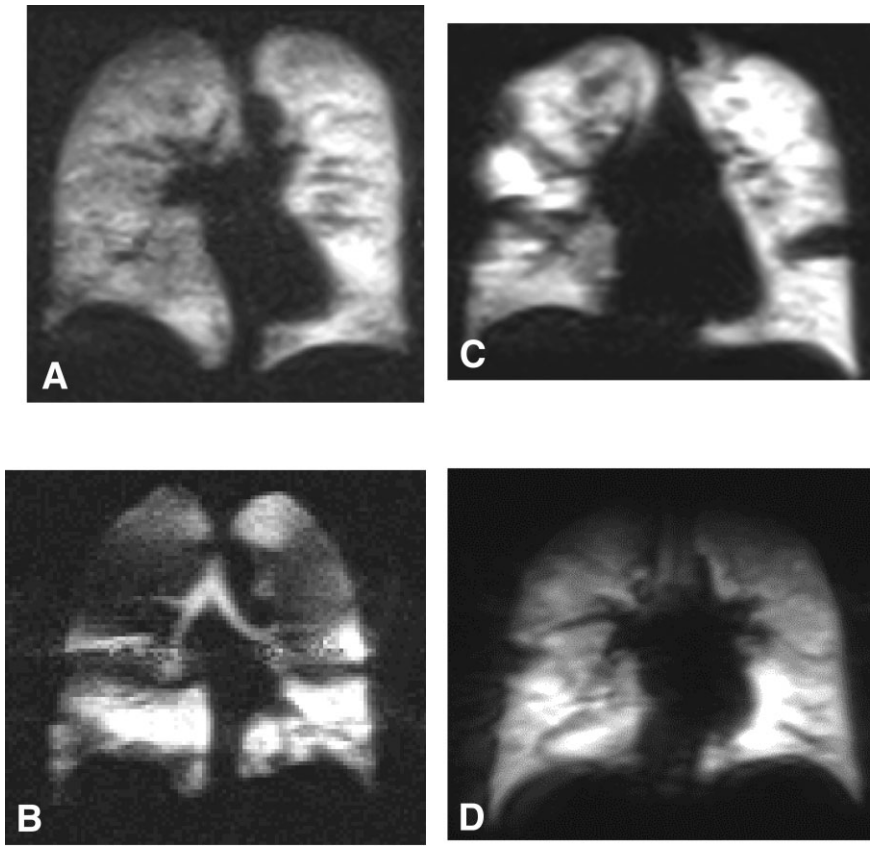

Figure 1. Coronal hyperpolarized 3-He MR ventilation distributionimage through the level of the carina in: normal volunteer (**A**), Patient with emphysema (**B**), nonsymptomatic smoker (**C**), and patient with asthma (**D**). The ability of the technique to diagnose obstruction in the peripheral airways is immediately apparent, with small wedge shaped ventilation defects visible in the asthmatic and smoker and large regions of impaired ventilation in the COPD patient. All of the images were acquired at 1.5 T during breath-hold of 200 mL of HP 3-He gas using a two-dimensional gradient echo sequence with a flip angle of 9°, 112 views, and 19 contiguous 10-mm coronal slices.

atoms takes on either an antiparallel or parallel (lower energy) state in relation to the strong magnetic field (B_0) within the MR environment. The net excess of spins occupying the lower energy state at a typical clinical field strength of 1.5 T is on the order of one in a million. In conventional proton MRI, the abundance of protons in the body compensates for this inherently low nuclear polarization. Unfortunately, noble gas nuclei demonstrate lower gyromagnetic ratios than protons and mostly have a much lower spin density, which limits the practicality of noble gas MR imaging based on the thermal-equilibrium spin population. Laser optical pumping techniques were developed over 50 years ago and have been used in a wide variety of applications in the field of physics research (11–13). This technology can potentially enhance the nuclear polarization by a factor of 100,000 compared to what is attainable in thermal equilibrium; this process is called hyperpolarization. Thus, although the overall spin density introduced into the lungs is low, the hyperpolarization compensates to give ample signal for MR imaging when the gas is inhaled.

Helium vs. Xenon

The first MR ventilation images in an animal were obtained using hyperpolarized 129-Xe (14), and this was soon followed by preliminary imaging and spectroscopy studies in animals and humans using both hyperpolarized 129-Xe (15–17) and 3-He (18–22). In subsequent years, hyperpolarized 3-He MR imaging became the topic of most intensive investigation and numerous papers were published. 3-He has become the most widely used gas for these studies, despite the fact that 129-Xe has a much higher natural abundance and is more widely available. This is because 3-He has certain physical properties that lend themselves to high signal-to-noise ratio (SNR) MRI; namely a larger gyromagnetic ratio ($\gamma_{3He} = 0.76\gamma_{1H}$ vs. $\gamma_{129xe} = 0.28\gamma_{1H}$) and the fact that polarization levels attainable to date with 3-He have generally been two to three times greater than those published for 129-Xe (23,24). However, 3-He has a larger diffusion coefficient than 129-Xe, meaning the MRI signal is more sensitive to attenuation by diffusion in applied gradients (25). There are also certain physiological issues relating to choice of HP noble gas; helium is virtually insoluble, meaning it is confined to the lung air-space during a breath-hold. Xenon is, however, highly soluble and can indeed be used to study gas exchange by perfusion. Once dissolved in the blood, its lypophilic nature means that xenon also has an anesthetic effect. The use of 129-Xe has much potential for studying gas exchange physiology and perfusion mechanisms, as xenon can be localized in the various phases of lung-to-blood transportation using spectroscopic methods. This review, however, focuses on the clinical applications of hyperpolarized 3-He MRI.

Production Methods

Comprehensive reviews of production methods for hyperpolarized 3-He have been published (26). Briefly, two methods are currently being used: spin-exchange optical pumping (27) and metastability exchange (12).

In both techniques, circularly polarized laser light is used, at the wavelength of the rubidium valence electron (795 nm) for spin exchange and helium (1083 nm) for metastability exchange.

Spin-exchange optical pumping has been developed into a stand-alone, commercial system for production of hyperpolarized 3-He at 30% to 50% polarization. Metastability exchange technology has been used in small systems (28–30), and has also been scaled up to a large central production facility. Because of the high polarization level achieved with the metastability exchange technique (>60%) and the availability of dedicated glass transportation containers having a T1 relaxation time of many hours, hyperpolarized 3-He can be distributed from a central production facility to a large geographic region (24,31,32). Thus, local production is feasible for institutions with sufficient manpower, expertise, and funding at the onset, while an on-demand method is available for institutions that do not have the technical know-how or resources available, yet wish to develop hyperpolarized 3-He MRI.

Technical Requirements for MR Imaging of Hyperpolarized 3-He

First, the MR system requires the appropriate hardware to transmit and receive at the Larmor frequency of helium, which is approximately 48 MHz at 1.5 T. A variety of radiofrequency (RF) coils have been used, such as birdcage, surface, and flexible-wrap coils (19,21–23, 32–37). Hyperpolarized 3-He lends itself to low field strength MR imaging because the polarization is independent of the field strength (38–42). Although lower field strengths have the advantage of reduced susceptibility artifacts, most of the developments of hyperpolarized 3-He MR imaging have made use of 1.5-T systems, as they are more widely available.

Imaging of inhaled hyperpolarized 3-He is limited by three main factors. First, the achieved polarization is "nonrenewable," meaning that some of the nonequilibrium magnetization is consumed during an acquisition; it can only be replenished by the introduction of additional hyperpolarized gas. This puts constraints on the pulse sequences employed, as discussed below. Second, the paramagnetic properties of oxygen in the airways lead to loss of polarization through T1 relaxation, which is dominated by the effects of oxygen in vivo. Third, the high diffusivity of helium (10^5 times larger than that of water) results in measurable signal loss even for the gradient waveforms used for routine imaging. Overall, sequence development has resulted in interesting and novel ways to ascertain aspects of lung function and morphology, as discussed below.

Delivery of Hyperpolarized Gas into the MR Environment

Once the 3-He gas has been polarized, it must be transported into the MR system without losing polarization. The most commonly applied methods either use a plastic bag (such as Tedlar, which is impermeable to 3-He and has a long surface T1) or a respirator-driven delivery system. The advantage of a bag is its simplicity, resulting in rapid insertion into the system and, additionally, its single-use; however, the disadvantages are that the bag method requires a single anoxic breathhold, which may pose problems for patients with severe lung diseases, and recycling (3-He is a limited resource) is more difficult to implement. The respirator-driven gas delivery system provides an accurate, individual dose that can be followed with an air chaser (no anoxic breath required) and that can be delivered within a chosen point of the respiratory cycle (43); these features permit standardization and individual quantification of gas delivery, and the closed configuration of the system makes recycling relatively straightforward to implement.

An important issue is the safety of 3-He delivery in human subjects with lung diseases. A recent assessment at the University of Virginia over a period of three years involving 343 subjects, ranging from normal volunteers to patients with severe lung disease, who inhaled more than 1000 doses of the gas (1 liter of anoxic gas using a Tedlar bag), revealed only mild adverse events in less than 10% of the subjects (44). Similar observations have been made at various other sites, indicating that inhalation of hyperpolarized 3-He gas is safe. The respirator-driven delivery system uses approximately 250 mL of 3-He gas as a bolus within a complete respiratory cycle, which includes a chaser of room air. The Tedlar bag method uses a maximum of 1 liter of a mixture of 300 mL 3-He and 700 mL N_2, and may be followed by an air chaser. Using these limited amounts of gas delivery appears to be safe, even in patients with more severe lung diseases, although minor desaturation for short time periods may occur. However, it should be stressed that these amounts should not be superseded, as the potential risks of a larger anoxic volume are considerable and could potentially lead to asphyxiation.

HYPERPOLARIZED 3-HELIUM MR IMAGING

The development of hyperpolarized 3-He MR imaging has led to four different techniques, each of which yields different information on lung function. The techniques developed are: static ventilation imaging (spin density), diffusion imaging (small airway size and configuration), dynamic ventilation imaging (gas in- and outflow), and oxygen partial pressure imaging (oxygen uptake or $\dot{V}Q$ matching). To understand how these techniques can improve our understanding of the pathophysiology of lung function, one must be aware of the available techniques for clinicians at present. Therefore, a brief summary of each of the four techniques follows.

Static Ventilation Imaging (Spin Density)

To effectively utilize finite hyperpolarization, low flip angles are required for pulse sequences that use multiple excitation RF pulses, and techniques such as two-dimensional–fast low angle single-shot (FLASH) have been adopted as the clinical gold standard so far (45). Nonetheless, prospective design of three-dimensional gradient echo sequences (46) has shown that SNR can

be improved, and therefore this approach is also worth consideration (Fig. 2). Modeling of these factors has demonstrated the effects on k-space filtering, the choice of flip angle, and the phase encoding strategy (25). Variable RF-pulse flip angles have also been used to provide the most efficient utilization of the nonequilibrium magnetization (47); however, this strategy requires very accurate calibration of the flip angle in vivo, which in turn requires the subject to inhale a separate calibration dose of gas. Recently, results were demonstrated using fast imaging with steady state free precession (FISP) gradient echo sequence, which could allow a more efficient use of polarization and an increased SNR (48). Alternatively, single-shot sequences have been implemented whereby all of the polarization is converted to transverse magnetization by a 90° RF pulse and k-space is rapidly encoded with echo planar imaging (EPI) (37). However, diffusion attenuation by the readout gradient waveform limits the spatial resolution with EPI at 1.5 T. At low field strength, single-shot fast spin echo or half-Fourier rapid acquisition with relaxation enhancement (RARE) sequences have been used successfully (41). Again, diffusion-induced signal loss is a particular concern for such single-shot techniques. Typically, approximately 15 slices are acquired during a single breath-hold of less than 20 seconds, resulting in images with a spatial resolution on the order of 2.5 × 2.5 × 10 mm. This is considerably better than lung scintigraphy, and the speed with which the images are obtained is also an advantage of 3-He imaging. With higher levels of gas polarization, further MR pulse sequence developments, and faster switching gradients, it is anticipated that the spatial resolution will be improved further.

Within spin density images, it is common to see areas that are better ventilated than others (Fig. 1). Generally, the distribution of 3-He has been observed to be gravity dependent, leading to increased signal intensity due to higher gas concentrations in the posterior and inferior lung zones with the subject in the supine position (49–51). An anterior–posterior change in the apparent diffusion coefficient (ADC) of the gas may also contribute to this anatomically related difference in SNR (46,52). Volume measurements can be performed, which have been shown to correlate well with pulmonary function tests, although reproducibility remains problematic (49,53). Indeed, care should be taken when inferring ventilation volume measurements from thick-slice gradient-echo images, as they are particularly susceptible to signal loss due to background field gradients, which could be misinterpreted as ventilation defects. Some of this signal loss can be restored by the application of an interleaved gradient-echo sequence with adjusted slice refocus gradients (54).

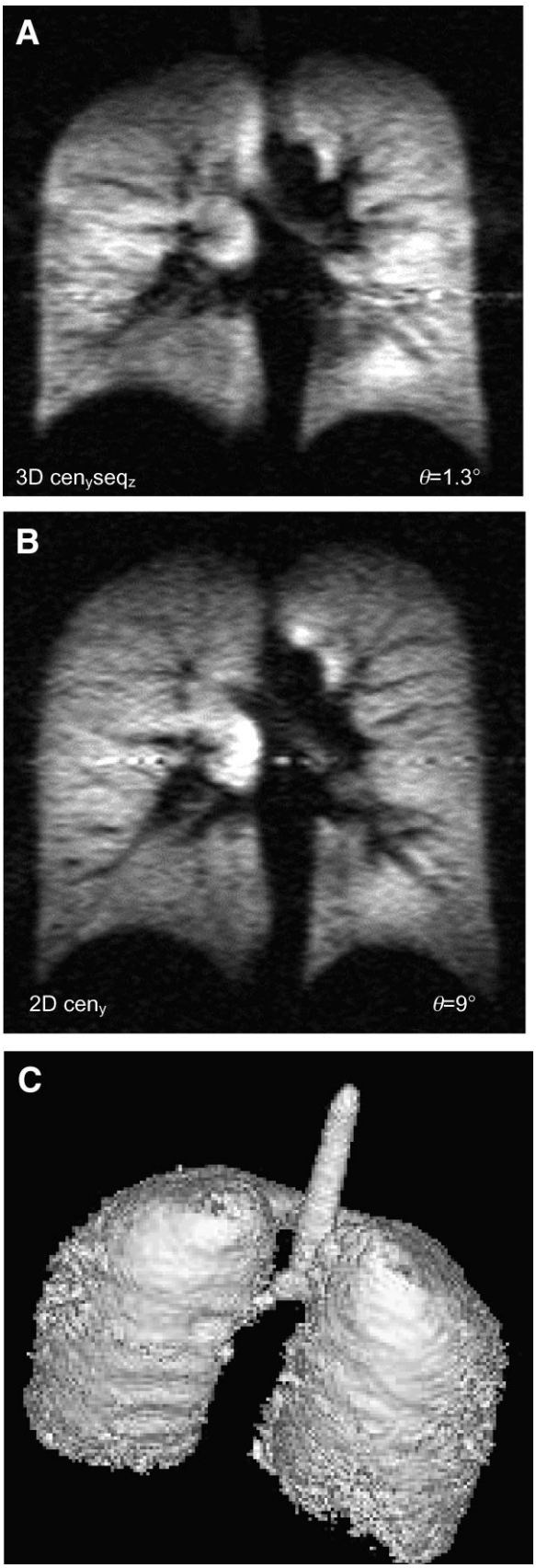

Figure 2. Images comparing the SNR and spatial resolution of three-dimensional and two-dimensional gradient echoes for imaging gas ventilation, using 300 mL of hyperpolarized 3-He. The three-dimensional acquisition (**A**) shows a higher SNR than the two-dimensional acquisition (**B**) with comparable spatial resolution. **C:** A volume rendering of ventilated lung volume obtained from the three-dimensional sequence with a nominal voxel size = 4.0 × 3.8 × 1.7 mm. The surface contours of the ribs and tracheal rings are visible, as is the peripheral ventilation defect in the posterior left lung. All images are from reference 46.

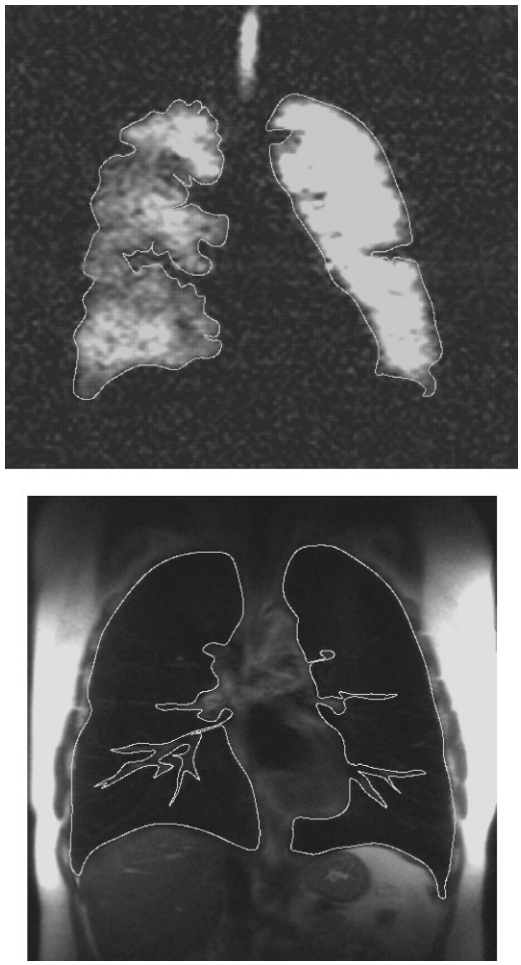

Figure 3. Method of quantification of ventilated lung volume. The lung is segmented in a proton MR image and the corresponding 3-He MR image is subsequently subtracted. This reveals the actual ventilated lung in this slice. Addition of slices yields the overall lung volumes.

A subtraction technique of calculated proton MR volumetry and hyperpolarized 3-He MR imaging, resulting in "effective ventilated lung volume" (Fig. 3), has recently been presented (55). This method is potentially useful, as it allows quantification of ventilation and thus the option to compare findings with subsequent follow-up investigations. However, most studies were performed in patients with only mild to moderate emphysema, so studies in more advanced disease are still required.

Dynamic Ventilation Imaging

Through the application of ultrafast pulse sequences, the respiratory cycle can be imaged using hyperpolarized 3-He MRI. The first published report of dynamic images in humans used a fast gradient-echo technique, thick slices in coronal orientation, and a temporal resolution of 1800 msec (21). Subsequently, by using an asymmetric echo and nonspatially-selective RF pulses, the acquisition time for a fast gradient-echo spin-warp pulse sequence was reduced to 130 msec for an image with 65 phase-encoding steps and permitted assessment of the in- and outflow of gas through the airways (56,57). Temporal resolution was increased further to 40 msec per image by using an EPI pulse sequence to image axial slices. EPI, however, can suffer from a degradation in spatial resolution (because of diffusion-induced signal loss) and an increase in susceptibility-related artifacts (37,58). An interleaved EPI pulse sequence (59) allowed the diffusion and susceptibility limitations to be reduced, but motion artifacts remained an issue (60). Nonetheless, this approach demonstrated homogeneous gas influx into the peripheral air spaces and confirmed the gravity dependence of gas inflow.

An alternative means of sampling k-space is offered by non-Cartesian strategies such as radial projection and spiral imaging. These approaches offer both central and peripheral sampling of k-space with each RF excitation. By using a "sliding window" reconstruction (61), these sampling strategies result in a smoother depiction of motion, with a higher refresh rate than that obtained with Cartesian-based sampling methods. Initial animal experiments showed promising results using both radial projection (62) and interleaved-spiral cine acquisitions (63) of inhaled 3-He gas.

The interleaved-spiral pulse sequence was further refined in human studies, allowing for an excellent compromise between temporal and spatial resolution, at a frame refreshment rate of 10 msec or less (64). The radial projection technique was also demonstrated in humans (Fig. 4), allowing for similar results at a refreshment rate of 4 msec (65). The information that can be obtained from these dynamic imaging techniques is capable of refining traditional lung function tests by providing quantitative measures of airflow on a regional basis (Fig. 4) (66,67).

More recently, it has been demonstrated with a fast gradient-echo pulse sequence that the contrast between the central airways and the peripheral air spaces can be manipulated by appropriate selection of the flip angle (68) and repetitive imaging on successive inhalations. By highlighting the appearance of airways down to a selected generation, it is thus possible to estimate the airways diameters.

Diffusion Imaging

An important property of 3-He is its extremely high self-diffusion coefficient (approximately 2 cm^2/seconds at body temperature and a pressure of 760 Torr). This property can be exploited in lung imaging, as diffusion becomes effectively restricted by the boundaries of the air spaces. Thus, the ADC (the diffusion measured within this restricted environment) effectively enables indirect assessment of the microstructure of the lung by measurement of the movement of the 3-He atoms.

Most 3-He ADC studies have used a gradient-echo pulse sequence, modified by the addition of a bipolar diffusion-sensitizing gradient waveform between the excitation RF pulse and data acquisition (69–74). By collecting two or more images at each section position with different diffusion weightings, parametric images of the ADC values can be calculated. Other methods for 3-He diffusion measurement have also been explored,

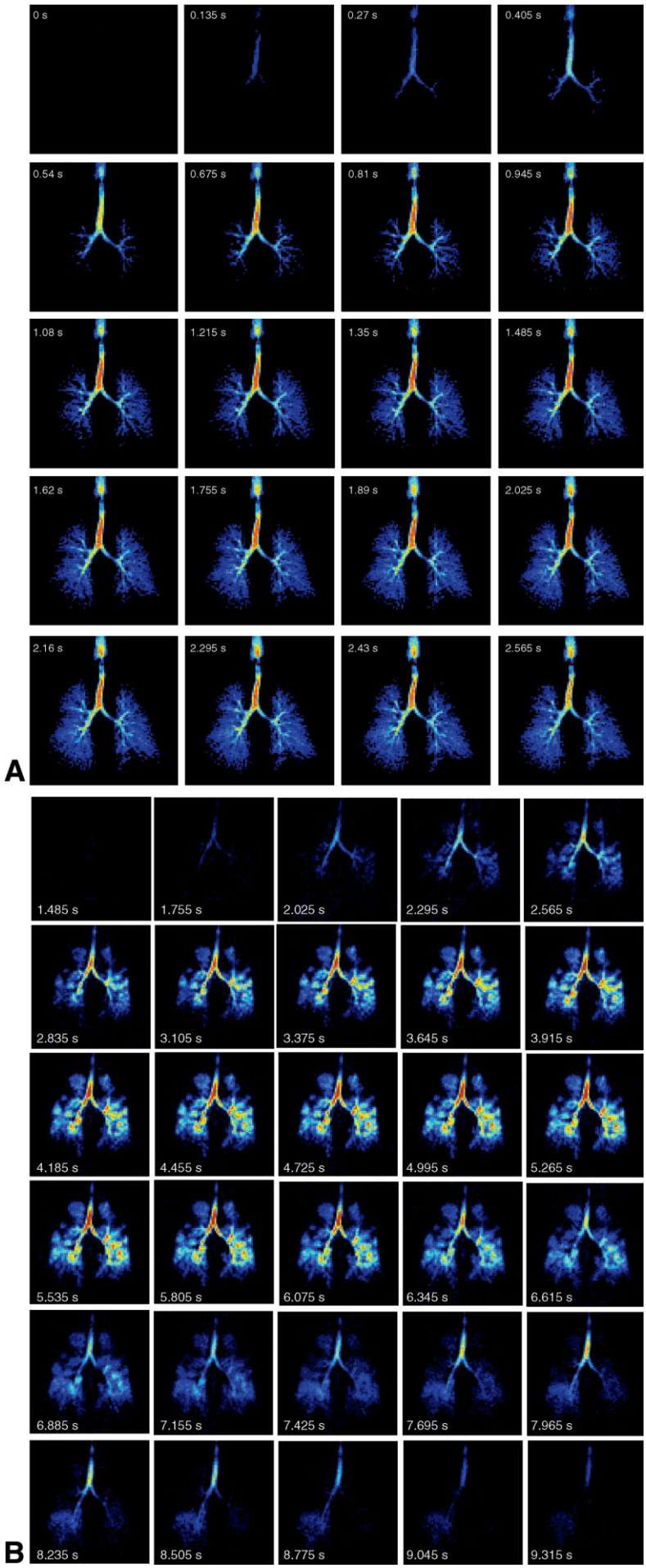

Figure 4. Dynamic images collected using a sliding window radial sequence (reference 65). **A:** Images from a healthy normal (128 views per frame) selected at intervals from the first part of an inhalation of 300 mL of 3-He polarized to 40%. The temporal passage of gas; down the trachea, into the bronchi and peripheral lung is clearly resolved. **B:** Dynamic time series from a COPD patient showing regions of ventilation obstruction in both lungs, particularly in the upper lobes and a delayed emptying/depolarization of gas in the lower left lobe, which could be indicative of air trapping.

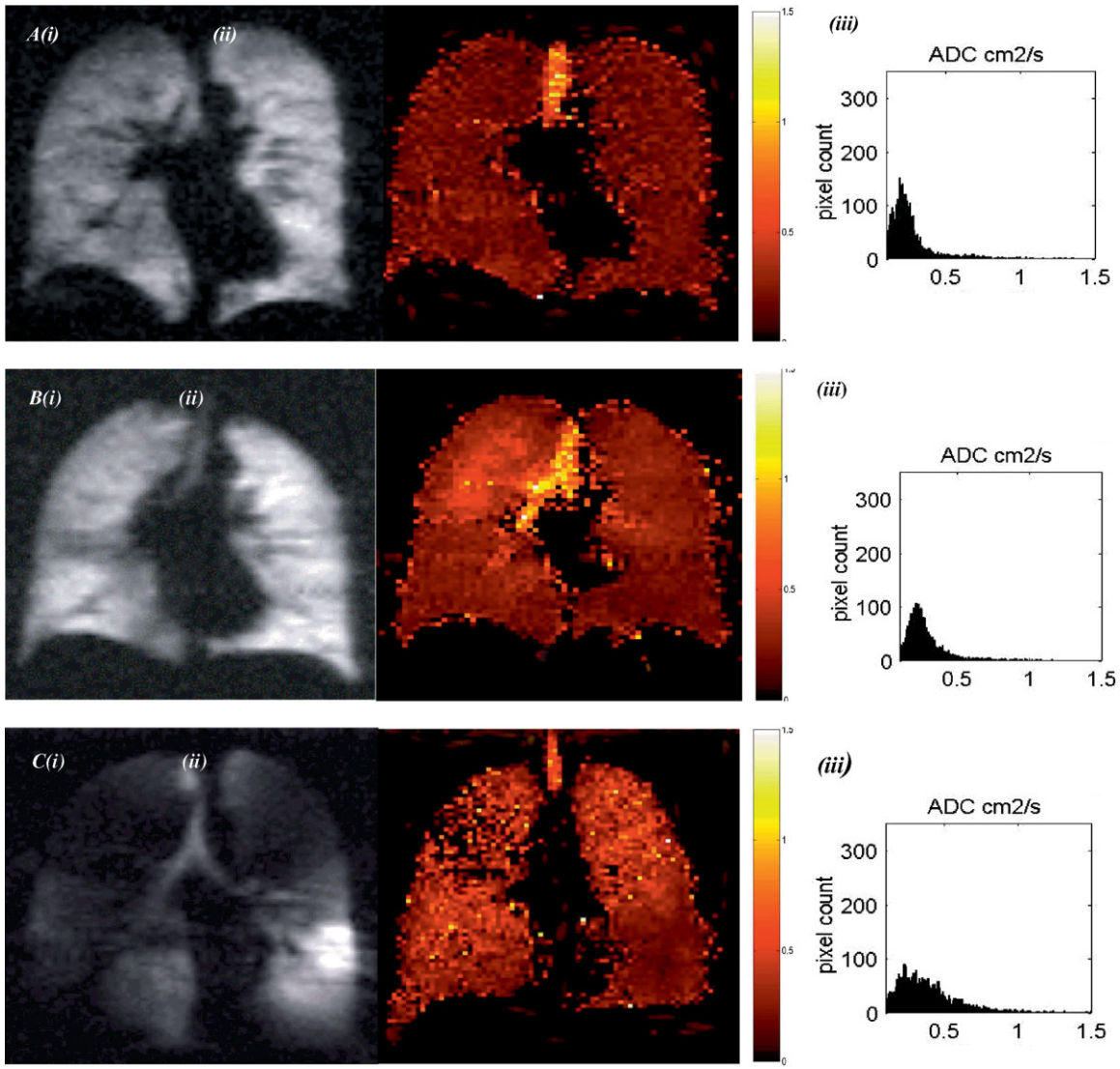

Figure 5. Ventilation distribution image, ADC map, and histogram of ADC values in normal volunteer (**A**), healthy smoker (**B**), and patient with emphysema (**C**).

including spin-echo-train pulse sequences (41) and magnetic-tag dissolution (75). There is some evidence to show that these techniques are more sensitive to gas diffusion over a longer length scale. The ADC measurement is typically depicted as an ADC map and histogram of ADC values (Fig. 5), which effectively yields information on the distribution of air space sizes and connectivity throughout the lungs (70–73).

Regional Oxygen Tension Imaging

The final step in the four-step protocol uses the paramagnetic effect of oxygen on the polarization of 3-He. In the presence of oxygen, the longitudinal relaxation of 3-He is accelerated (76). However, depolarization also occurs as a direct result of the application of RF pulses. Subsequent studies in large animals and humans have demonstrated that it is possible to correct for RF-pulse effects, revealing that the oxygen-induced signal decay rate is linearly proportional to the concentration of oxygen (43). Using two breath-holds with different flip angles and/or interscan delays for the acquisitions occurring during each breath hold, it is possible to determine regional intrapulmonary oxygen partial pressure (pO_2) within 95% accuracy and at an in-plane resolution of 1×1 cm (77). This technique was further refined by using a single-acquisition, single breath-hold technique, which has improved temporal resolution (15 seconds) and reduced error because the need for a second breath hold, which may be in a different position than the first, is eliminated (78). Thus, the regional oxygen concentration in the airways can be depicted (Fig. 6), and from its variation along time, the regional oxygen uptake can be inferred (43,77,78). Oxygen uptake is dependent on lung perfusion, and thus the map can be seen as a regional ventilation perfusion (V_A/Q) map of the lung (78), allowing, for the first time, a direct measurement of the regional V_A/Q distribution in a noninvasive fashion at relatively high resolution when compared to ventilation perfusion scintigraphy. More recently this methodology previously applied with a

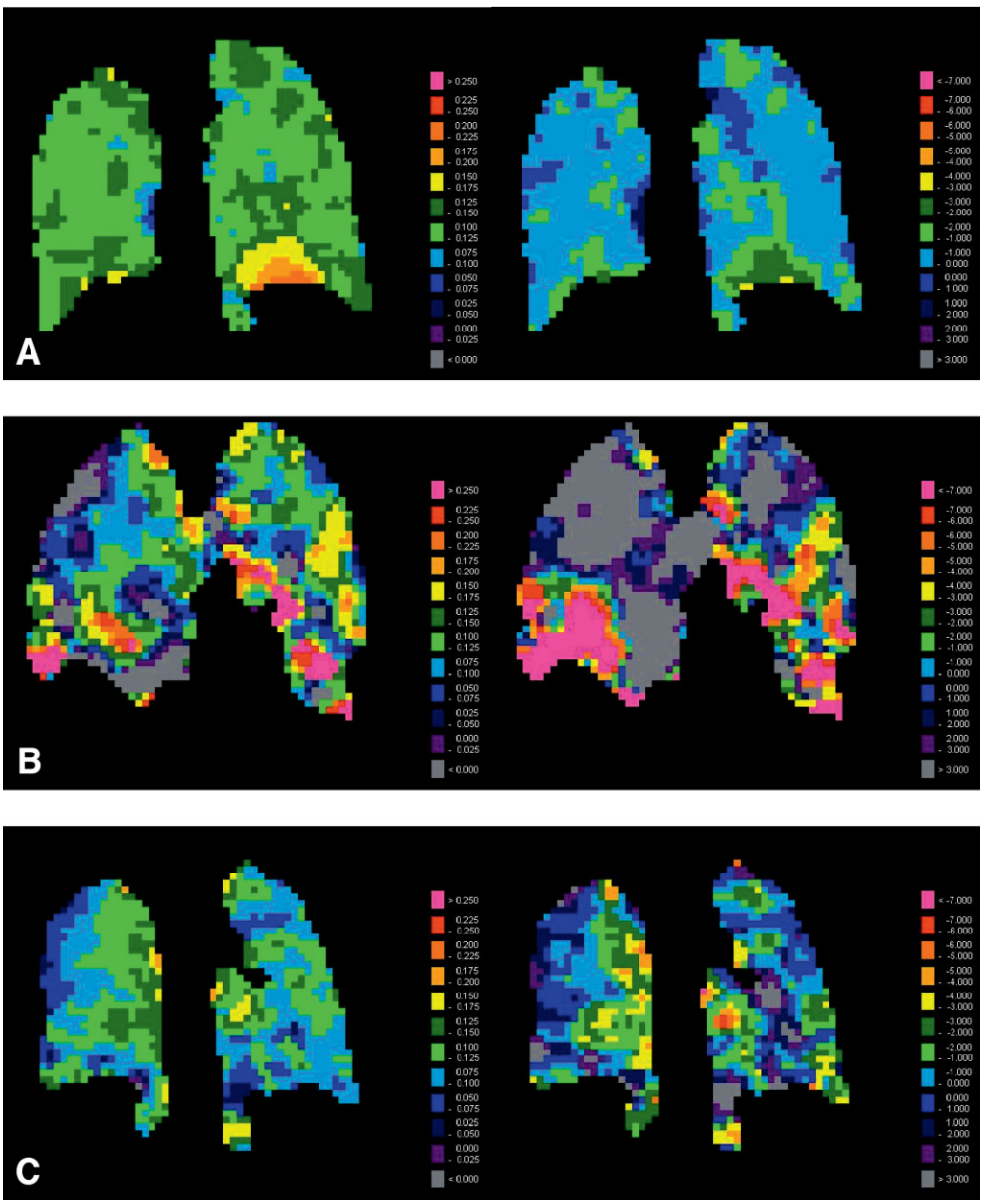

Figure 6. Oxygen-sensitive MR map (left) with correlating maps of oxygen decrease rates (right) obtained during a single breath-hold in: normal volunteer (**A**), patient with emphysema (**B**), and patient with chronic thromboembolic pulmonary hypertension (**C**).

two-dimensional whole lung projection has been adapted for use with three-dimensional gradient echo sequences (46), thus providing accurate depiction of pO_2 at a higher spatial resolution in three dimensions (Fig. 7).

CLINICAL APPLICATIONS

Due to the relatively recent introduction of hyperpolarized 3-He MR imaging of the lung, experience with this technology is still limited, with approximately 500–1000 subjects studied worldwide, and all studies have been performed on an investigational basis. However, the initial results have been encouraging, suggesting that the integration of functional and morphological data required for treatment planning and assessment of treatment effectiveness may be achieved. One of the main advantages is, of course, that the technique appears safe, is noninvasive and reproducible, and does not require ionizing radiation. This makes it an interesting tool for application in longitudinal or follow-up studies, in which multiple assessments may be required. Several areas have been investigated thus far (examples are given in the figures), and these will now be discussed.

The Normal, Healthy Lung

Numerous studies in normal volunteers have shown that a single inhalation of hyperpolarized helium-3 gas is sufficient to fill all alveolar spaces, providing homogeneous distribution of the signal throughout the lungs. The rapid distribution of the gas is not unexpected, as helium gas diffuses quickly (approximately 1 mm/msec). Typically, the pulmonary vessels are seen as linear, low intensity structures radiating from the hilar areas. On occasion, small ventilation defects are seen in normal subjects. It has been demonstrated that prolonged immobilization

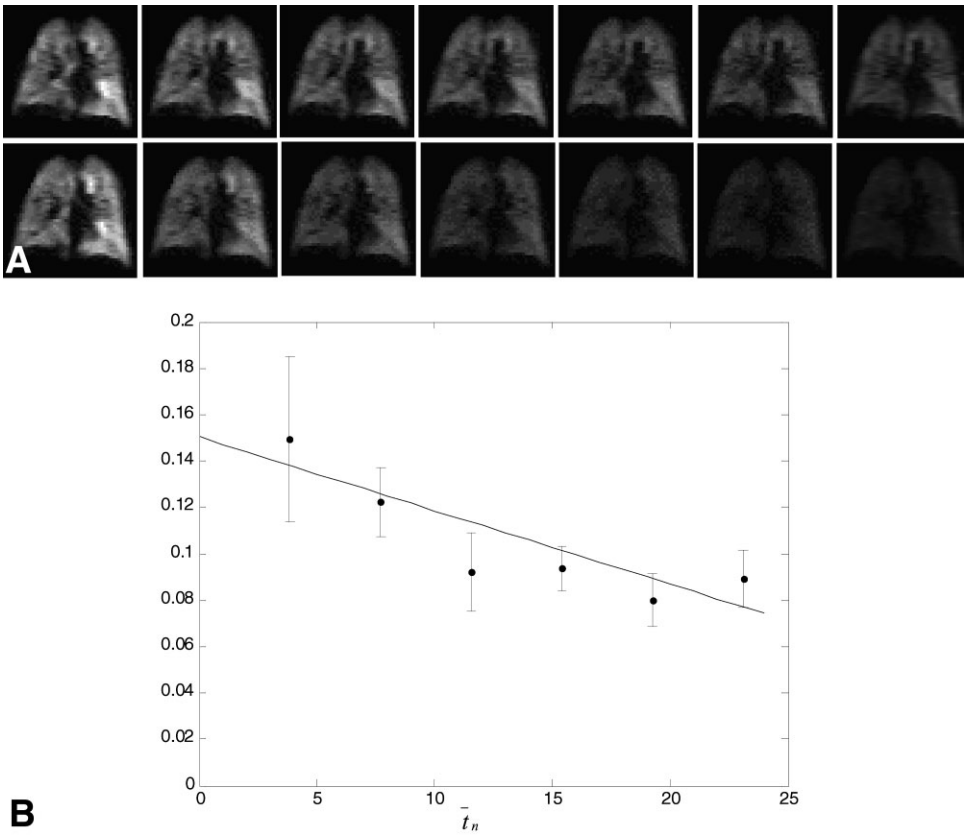

Figure 7. Volume localized measurement of pO_2 with three-dimensional gradient echo imaging sequence (reference 46). **A:** The two time series of images from an in vivo study on a healthy normal. The images from the short delay (τ_1 = 1.7 seconds) time series are shown in the top row. The bottom row represents the longer delay series (τ_2 = 6 seconds). **B:** The pO_2 as measured from the ROI in the lower right lung (see Fig. 3A). The y-axis intercept of the fitted curve gives the initial p_0 = 0.147 bar and the slope R = 0.003 bar/second.

may lead to a significant increase in the number of defects and development of new ones, particularly in the dependent portions of the lung (79). These defects are believed to be caused by small foci of atelectasis that are induced by prolonged immobilization, similar to what has been observed during CT scanning (80). Indeed, a study using 3-He ADC in various positions showed that airspaces decrease in size in dependent portions of the lung and that the weight of the heart also has a significant influence in this process (52). Since there are no specific imaging features that allow distinction between the immobilization-induced and disease-related hyperpolarized 3-He ventilation defects, it is important that MR imaging is performed quickly after the subject is positioned on the scanner table in order to prevent the development of these abnormalities.

Chronic Obstructive Pulmonary Diseases

Chronic obstructive pulmonary diseases (COPDs) are lung diseases that are characterized by obstruction of airflow and air trapping. COPD affects over 11 million people in the United States alone, and 3.1 million of these suffer from emphysema (81). Emphysema is histopathologically defined as the abnormal, permanent enlargement of the airspaces distal to the terminal bronchioles, accompanied by destruction of their walls without obvious fibrosis (82). Factors associated with emphysema are smoking, aging, inherited alpha-1-antitrypsin deficiency, and toxic gases in industrial settings.

Several studies have shown that the size and extent of ventilation defects as demonstrated by 3-He MRI correlates well with spirometry (21,22,36,49,58).

In addition to ventilation distribution, ADC measurements in subjects with COPD have been shown to be capable of distinguishing between normal lung and emphysema (72,73). Thus, this technique can be employed to distinguish areas within the lung that are affected to a greater or lesser extent by the disease (Fig. 5). A drawback of ADC maps is that the data for calculating these maps can only be derived in ventilated lung areas. Thus, ADC maps will have to be interpreted in conjunction with ventilation distribution images. Furthermore, posture and gravity appear to affect the ADC values, which is relevant, as most studies are performed with the patient supine (52). The effect of gravity on ADC measurements could potentially be resolved by novel MR system designs.

Dynamic ventilation techniques are capable of demonstrating airflow abnormalities (64–67). One recent study was able to demonstrate delayed outflow of 3-He gas in subjects with COPD, thought to reflect the presence of air trapping within the lung (Fig. 4) (83).

The future role of hyperpolarized 3-He MRI in the context of COPD is still under discussion. Anticipated applications include the pre- and postoperative assessment of patients who undergo lung volume reduction surgery, the early diagnosis of COPD, and use in therapy trials to assess effectiveness of new medications.

Smoker's Lungs

The effects of smoking on the lungs are manifold, including increased mucus production and enzymatic changes. The effects initially involve small airways, but chronic changes also involve the major airways.

Chronic obstruction of the small airways leads to bronchiolitis, while enzymatic and toxic changes result in destruction of alveolar walls and emphysema. Most studies in emphysema using hyperpolarized 3-He MR imaging were performed in patients with smoking related lung diseases (as described above).

A study comparing the number and size of ventilation defects in seven smokers and five nonsmokers with normal mean forced expiratory volume in 1 second (84) showed that there was a greater number of defects in the smokers, and these defects were also more extensive than those seen in nonsmokers. Another study also showed there was a correlation between the extent of 3-He ventilation defects and smoking history, and extent of emphysema (36). A study comparing quantitative 3-He and proton lung volumes (Fig. 3) in seven smokers and six nonsmokers demonstrated a 37% reduction of ventilated lung volume in smokers and a 12% reduction in ventilated lung volume in nonsmokers (55). These studies suggest that early detection of lung damage due to smoking may be possible with 3-He MR imaging and that the extent of disease (and possible progression or treatment effects) may be quantifiable (85,86).

Cystic Fibrosis and Bronchiectasis

Cystic fibrosis (CF) is an inherited disorder, which traditionally leads to early death. The introduction of screening programs and supportive therapies, such as antibiotic prophylaxis, mucolytics, physiotherapy, and enzyme substitution therapy, has improved survival beyond the age of 30 years. Image scoring systems have been used clinically and as objective measurement tools for assessment of therapeutic effects in research trials for CF (87,88). Both high resolution computed tomography (HRCT) (87,88) and nuclear medicine techniques (89) have been shown to give useful information, but for fear of cumulative radiation doses, they are not uniformly used, and evaluation of lung function in patients with CF is largely limited to chest radiography and pulmonary function tests with the latter providing global information of the lung.

CF causes nonuniform changes in the lungs, and information on the site(s) of disease could have an effect on treatment. Because the introduction of screening programs has led to early intervention in CF, the damage to the lung may be minimal, which makes assessing the effects of therapy more difficult. Chest radiography and lung function tests will probably not yield sufficient discriminatory value to determine whether new treatments are effective, as these tests are relatively insensitive to subtle changes. Thus, it seems of utmost importance to develop novel techniques, which have no ionizing radiation burden, and which can provide regional lung function data.

An initial study in four adult subjects with CF demonstrated good acceptance of the 3-He MR imaging technique (90). Widespread ventilation defects were observed in all subjects, with a predominance in the upper lung zones. There was good correlation between the extent of ventilation defects and pulmonary function tests. A second study in three subjects with CF, comparing 3-He MR imaging with spirometry before and after mucus clearance therapy (91), showed good correlation between 3-He MR imaging findings and spirometry before therapy. In two of the three subjects who underwent a second MR examination immediately following therapy for mucus clearance, spirometry only improved slightly in one, whereas a significant decrease in ventilation defects was demonstrated in both. This finding would suggest greater sensitivity of 3-He MRI than spirometry in this setting.

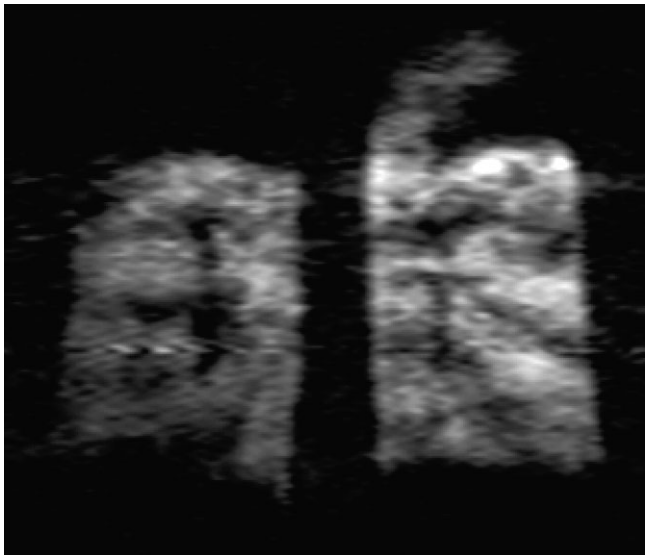

Figure 8. Ventilation distribution images in a child with cystic fibrosis. Note the upper lobe predominance of the disease.

More recent experience in eight children with CF (age range 6–15 years) also demonstrated good acceptance of the technique (92). Ventilation defects correlated well with spirometry findings, and in two children with antibiotic-resistant *Pseudomonas aeruginosa* infection, the defects were more extensive in the upper lobes compared to the subjects without resistant infection (Fig. 8). Moreover, the MRI scores correlated better with functional data than chest radiology scores.

Asthma

Asthma is a chronic disease that affects large numbers of predominantly young people. It is defined as a combination of reversible small airway obstruction, inflammation, and increased airway responsiveness (93). Spirometry is the mainstay of management, but its sensitivity for early detection of airway inflammation has been questioned. Furthermore, regional differences cannot be evaluated using standard techniques.

The role of imaging has been limited, and chest radiographs tend to be normal in uncomplicated cases (94). During acute asthma episodes, hyperinflation and thickened bronchi are present in up to 40% of patients (95). HRCT is more sensitive in depicting air trapping and bronchial wall thickening, but the correlation with disease severity is questionable (96,97).

Hyperpolarized 3-He studies have demonstrated that various degrees of ventilation defects are detectable in asthma and that small ventilation defects also vary in

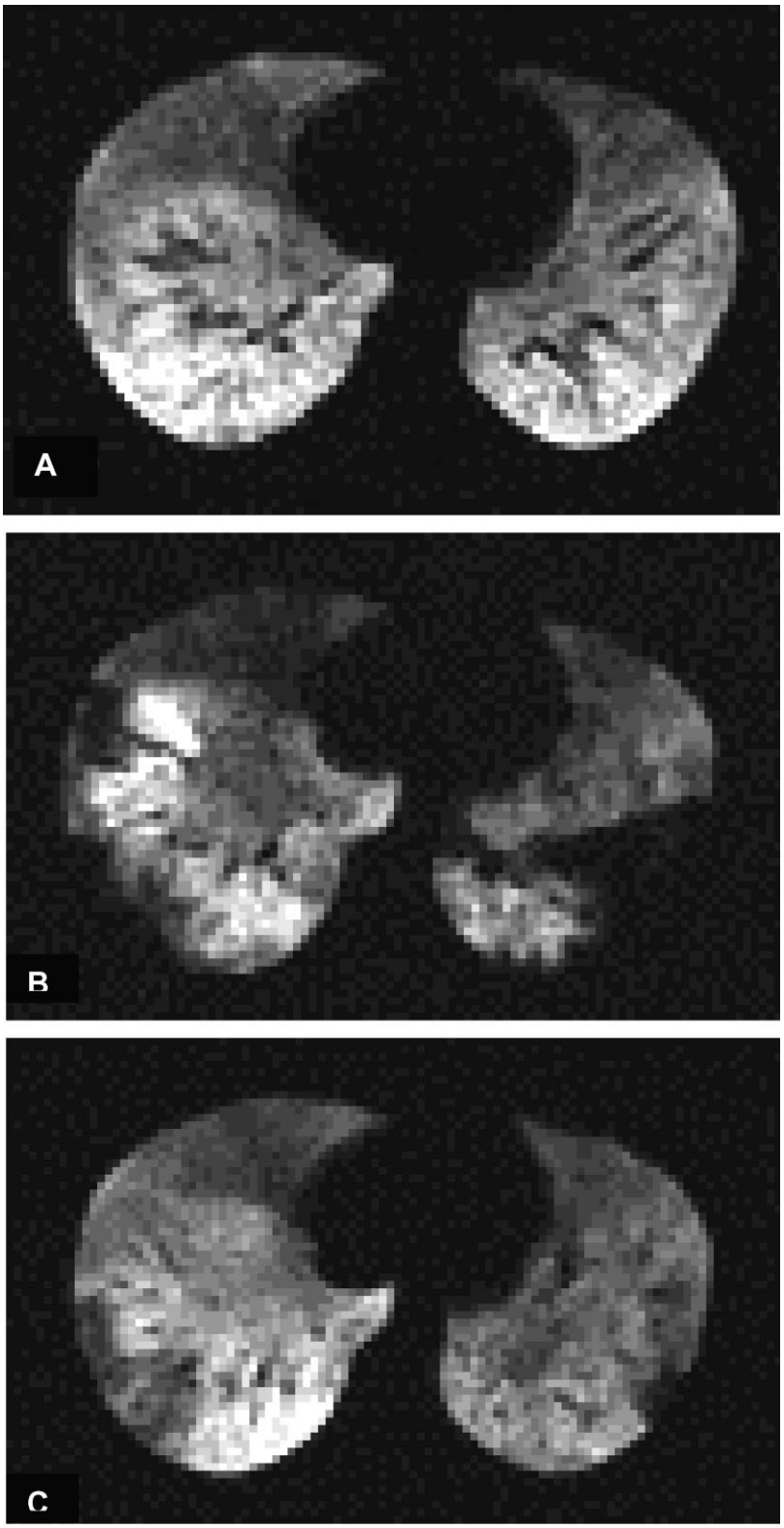

Figure 9. Axial hyperpolarized 3-He MR ventilation images of a patient with asthma, who was given methacholine. **A:** At baseline the subject had normal spirometry findings (FEV_1 100% of predicted) and the lungs showed normal, homogeneous distribution of the signal. **B:** Immediately after methacholine challenge, the lung function decreased (FEV_1 75% of predicted) and there were extensive ventilation defects in the lungs. **C:** One hour later, there was improvement of the spirometry findings (FEV_1 85% of predicted) and most of the defects had resolved, with only few remaining.

location over time. In a study that compared 10 healthy volunteers with 10 asthmatics, seven of the asthmatics had (generally small) ventilation defects distributed throughout the lungs, while no defects were present in the normal controls. Two symptomatic patients had larger and a greater number of ventilation defects. One subject who was studied after three weeks demonstrated resolution of the defects, while another subject showed resolution of defects following bronchodilator therapy (98). It was, however, not possible to conclusively define the severity of asthma, as reported by patients, based on the findings of hyperpolarized 3-He MRI (99). Nevertheless, good correlation was demonstrated between MRI and spirometry, which possibly

demonstrates that objective findings are not necessarily linked to subjective well-being.

In another study in six subjects with exercise-induced asthma, four subjects with ventilation defects and normal spirometry at baseline demonstrated ventilation defects that changed in size and location following methacholine challenge (Fig. 9) (100). Overall, the number and size of defects increased in parallel to a decrease in lung function. More recently, a study in nine asthmatics and two healthy volunteers demonstrated that both exercise and methacholine challenge induced, on the average, a three-fold increase in the percentage of nonventilated lung (101). Furthermore, a study in one subject demonstrated that it is feasible to detect airway caliber changes following methacholine challenge (102).

It can be deduced that hyperpolarized 3-He MR imaging has the potential to provide direct visualization of the ventilatory changes in the lung that cause the pulmonary functional impairment characterizing asthma. The technique appears to be particularly sensitive for small airways changes and is capable of demonstrating the response to both challenges and therapy.

Lung Transplant (Bronchiolitis Obliterans)

The main reason for failure of lung transplantation is a chronic host vs. graft reaction, which manifests itself as bronchiolitis obliterans (103). Early diagnosis is paramount, as an increase in immunosuppressive therapy is required. However, early diagnosis is also difficult due to the inhomogeneous distribution of the disease, which can lead to underestimation of disease when a relatively normal section of the lung is biopsied using bronchoscopy. As hyperpolarized 3-He MR imaging appears to be sensitive in detecting areas of abnormal ventilation in the transplanted lung, the technique may assisting with management by guiding the biopsy.

An initial study in six lung transplant patients compared the findings of 3-He MR imaging with a clinical grading system for bronchiolitis obliterans (104). Focal ventilation defects were present in all patients, and the defects were more extensive than those on corresponding 133-Xe scintigraphy (two patients) and HRCT (three patients). The 3-He MR imaging findings correlated well with the clinical grading system.

Another study in 14 lung transplant patients compared the hyperpolarized 3-He MR findings with HRCT (105). A total of 59 ventilation defects were demonstrated and only 63% of these correlated with focal CT findings (Fig. 10). This study suggests that 3-He MRI is more sensitive for the detection of ventilation abnormalities than HRCT, and therefore that it may provide earlier detection of bronchiolitis obliterans.

A more recent study compared hyperpolarized 3-He MR imaging with spirometry forced expiratory volume in 1 second (FEV_1) in nine patients following single- or double-lung transplant for either emphysema or idiopathic pulmonary fibrosis (106). Decrease in the ventilated volume of the lung graft as demonstrated by hyperpolarized 3-He MRI correlated well with the degree of bronchiolitis obliterans. In addition, it was found that the changes demonstrated by 3-He MR imaging were seen before changes in spirometry became evident. Furthermore, one study used dynamic imaging to detect airflow changes as a possible early marker of lung rejection in lung transplant patients (107). These studies suggest that hyperpolarized 3-He MR imaging could have a role in the management of patients following lung transplantation.

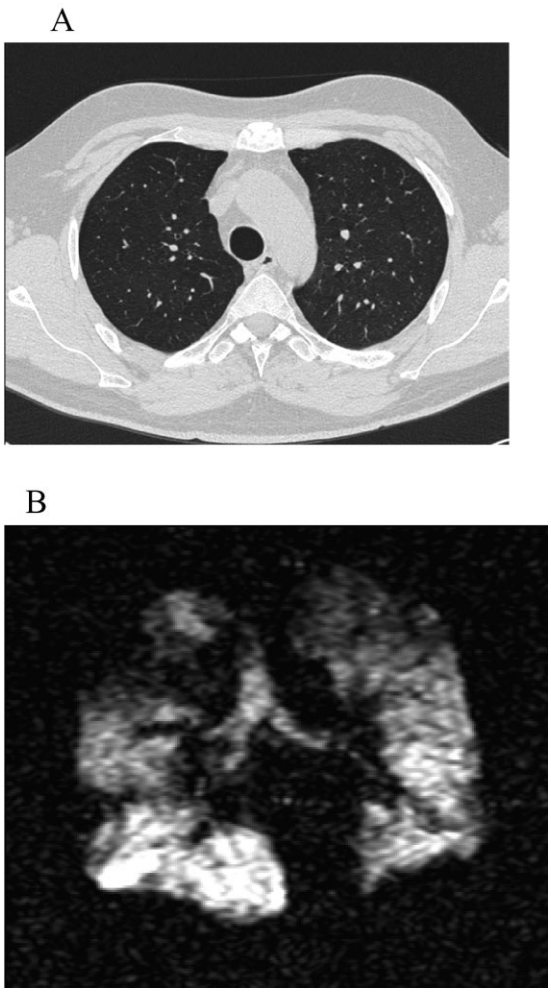

Figure 10. Comparative images in a patient with subsequently proven bronchiolitis obliterans. **A:** HRCT image demonstrating normal lung parenchyma. **B:** Corresponding hyperpolarized 3-He MR image with ventilation defects.

Pulmonary Embolism

Pulmonary embolism is a common clinical condition, and the use of MR techniques for detection of this condition was recently described in this journal (9). Although acute pulmonary embolism could be diagnosed using a combination of perfusion and ventilation MR imaging, it is unlikely that this approach would find routine implementation due to the technical requirements and the fact that MRI may be less readily available compared to multidetector CT. However, the application of hyperpolarized 3-He MR in chronic thromboembolic pulmonary hypertension may be relevant, as the technique is capable of providing information about the ventilation perfusion mismatch and ox-

ygen uptake of the lung (43,77,78). Knowledge of these basic pulmonary function parameters could prove helpful in planning therapy, both from a medical and surgical point of view. Furthermore, the information provided by this technique may allow a more comprehensive noninvasive diagnostic work-up of these patients than is currently possible. To date, no studies in humans to assess the value of this technology have been performed, other than those performed to validate the technique of 3-He–based oxygen tension imaging as discussed above (77,78).

CONCLUSIONS

Hyperpolarized 3-He MR imaging of the lungs is capable of demonstrating pathophysiological changes. It permits noninvasive assessment and provides regional information on both lung morphology and function. It is expected that this technology will find its way into routine clinical use to evaluate a variety of lung diseases, in particular those that are difficult to assess using currently available diagnostic methods. Furthermore, it is likely that the technology will become a useful tool for providing an insight into the action and effectiveness of therapeutic interventions of the lung.

ACKNOWLEDGMENTS

We thank Amersham Health (for the loan of polarizer equipment) and Spectra Gases (for technical support).

REFERENCES

1. Lucidarme O, Coche E, Cluzel P, et al. Expiratory CT scans for chronic airway disease: correlation with pulmonary function test results. AJR Am J Roentgenol 1998;170:301–307.
2. Park CS, Müller NL, Worthy SA, et al. Airway obstruction in asthmatic and healthy individuals: inspiratory and expiratory thin-section CT findings. Radiology 1997;203:361–367.
3. Hu S, Hoffman EA, Reinhardt JM. Automatic lung segmentation for accurate quantitation of volumetric X-ray CT images. IEEE Trans Med Imaging 2001;20:490–498.
4. Park KJ, Bergin CJ, Clausen JL. Quantitation of emphysema with three-dimensional CT densitometry: comparison with two-dimensional analysis, visual emphysema scores, and pulmonary function test results. Radiology 1999;211:541–547.
5. Tajik JK, Chon D, Won C, Tran BQ, Hoffman EA. Subsecond multisection CT of regional pulmonary ventilation. Acad Radiol 2002;9:130–146.
6. Almquist H, Jonson B, Palmer J, Valind S, Wollmer P. Regional VA/Q ratios in man using 133Xe and single photon emission computed tomography (SPECT) corrected for attenuation. Clin Physiol 1999;19:475–481.
7. Sanchez-Crespo A, Petersson J, Nyren S, et al. A novel quantitative dual-isotope method for simultaneous ventilation and perfusion SPET. Eur J Nucl Med Mol Imaging 2002;29:863–875.
8. Suga K, Tsukuda T, Awaya H, Matsunaga N, Sugi K, Esato K. Interactions of regional respiratory mechanics and pulmonary ventilatory impairment in pulmonary emphysema: assessment with dynamic MRI and xenon-133 single-photon emission CT. Chest 2000;117:1646–1655.
9. van Beek EJR, Wild JM, Fink C, Moody AR, Kauczor HU, Oudkerk M. MRI for the diagnosis of venous thromboembolic disease. J Magn Reson Imaging 2003;18:627–640.
10. Moller HE, Chen XJ, Saam B, et al. MRI of the lungs using hyperpolarized noble gases. Magn Reson Med 2002;47:1029–1051.
11. Kastler A. Quelques suggestions concernant la production optique et la detection optique d'une inégalité de population des niveaux de quantification spatiale des atomes. Application à l'expérience de Stern et Gerlach et à la resonance magnétique. J Phys Radium 1950;11:255–265. [Fre]
12. Colegrove FD, Schearer LD Walters GK. Polarisation of He3 gas by optical pumping. Phys Rev 1963;132:2561–2572.
13. Miron E, Schaefer S, Schreiber D, Van Wijngaarden WA, Zeng X, Happer W. Polarisation of the nuclear spins of noble-gas atoms by spin exchange with optically pumped alkali-metal atoms. Phys Rev A Gen Phys 1984;29:3092–3110.
14. Albert MS, Cates GD, Driehuys B, et al. Biological magnetic resonance imaging using laser-polarized 129Xe. Nature 1994;370:199–201.
15. Wagshul ME, Button TM, Li HF, et al. In vivo MR imaging and spectroscopy using hyperpolarized 129Xe. Magn Reson Med 1996;36:183–191.
16. Sakai K, Bilek AM, Oteiza E, et al. Temporal dynamics of hyperpolarized 129Xe resonances in living rats. J Magn Reson B 1996;111:300–304.
17. Mugler III JP, Driehuys B, Brookeman JR, et al. MR imaging and spectroscopy using hyperpolarized 129Xe gas: preliminary human results. Magn Reson Med 1997;37:809–815.
18. Middleton H, Black RD, Saam B, et al. MR imaging with hyperpolarized 3He gas. Magn Reson Med 1995;33:271–275.
19. Black RD, Middleton HD, Cates GD, et al. In vivo He-3 MR images of guinea pig lungs. Radiology 1996;199:867–870.
20. Ebert M, Großmann T, Heil W, et al. Nuclear magnetic resonance imaging on humans using hyperpolarised 3He. Lancet 1996;347:1297–1299.
21. MacFall JR, Charles HC, Black RD, et al. Human lung air spaces: potential for MR imaging with hyperpolarized He-3. Radiology 1996;200:553–558.
22. Kauczor HU, Hofmann D, Kreitner KF, et al. Normal and abnormal pulmonary ventilation: visualization at hyperpolarized He-3 MR imaging. Radiology 1996;201:564–568.
23. Driehuys B, Cates GD, Miron E, Sauer K, Walter DK, Happer W. High-volume production of laser-polarized 129Xe. Appl Phys Lett 1996;69:1668–1670.
24. Becker J, Heil W, Krug B, et al. Study of mechanical compression of spin-polarized 3He gas. Nucl Instrum Meth A 1994;346:45–51.
25. Wild JM, Paley MNH, Viallon M, Schreiber WG, van Beek EJR, Griffiths PD. K-Space filtering in 2D gradient echo breath-hold hyperpolarized 3He MRI: spatial resolution and signal to noise considerations. Magn Res Med 2002;47:687–695.
26. Goodson BM. Nuclear magnetic resonance of laser-polarized noble gases in molecules, materials, and organisms. J Magn Reson 2002;155:157–216.
27. Bouchiat MA, Carver TR, Varnum CM. Nuclear polarisation in 3He gas induced by optical pumping and dipolar exchange. Phys Rev Lett 1960;5:373–375.
28. Candela D, Hayden ME, Nacher PJ. Steady-state production of high nuclear polarization in 3He-4He mixtures. Phys Rev Lett 1994;73:2587–2590.
29. Nacher PJ, Tastevin G, Maître X, Dollat X, Lemaire B, Olejnik J. A peristaltic compressor for hyperpolarized helium. Eur Radiol 1999;9:B18.
30. Gentile TR, Jones GL, Thompson AK, et al. Demonstration of a compact compressor for application of metastability-exchange optical pumping of 3He to human lung imaging. Magn Reson Med 2000;43:290–294.
31. Heil W, Humblot, Otten EW, Schafer M, Surkau R, Leduc M. Very long nuclear relaxation times of spin polarized helium-3 in metal coated cells. Phys Lett A 1995;201:337–343.
32. Wild JM, Schmiedeskamp J, Paley MNJ, et al. MR imaging of the lungs with hyperpolarized 3-Helium transported by air. Phys Med Biol 2002;47:N185–N190.
33. Johnson GA, Cates G, Chen XJ, et al. Dynamics of magnetization in hyperpolarized gas MRI of the lung. Magn Reson Med 1997;38:66–71.
34. Walker TG, Happer W. Spin-exchange optical pumping of noble-gas nuclei. Rev Mod Phys 1997;69:629–642.
35. Darrasse L, Guillot G, Nacher PJ, Tastevin G. Low-field 3He nuclear magnetic resonance in human lungs. C R Acad Sci II B 1997;324:691–700.
36. de Lange EE, Mugler III JP, Brookeman JR, et al. Lung air spaces: MR imaging evaluation with hyperpolarized 3He gas. Radiology 1999;210:851–857.

37. Saam B, Yablonskiy DA, Gierada DS, Conradi MS. Rapid imaging of hyperpolarized gas using EPI. Magn Reson Med 1999;42:507–514.
38. Tseng CH, Wong GP, Pomeroy VR, et al. Low-field MRI of laser polarized noble gas. Phys Rev Lett 1998;26;81:3785–3788.
39. Wong GP, Tseng CH, Pomeroy VR, et al. A system for low field imaging of laser-polarized noble gas. J Magn Reson 1999;141: 217–227.
40. McGloin C, Benattayallah A, Bowtell RW, et al. Low field lung imaging using hyperpolarized 3He. In: Proceedings of the 9th Annual Meeting of ISMRM, Glasgow, Scotland, 2001. (abstract 947).
41. Durand E, Guillot G, Darrasse L, et al. CPMG measurements and ultrafast imaging in human lungs with hyperpolarized helium-3 at low field (0.1 T). Magn Reson Med 2002;47:75–81.
42. Bidinosti CB, Choukeife J, Nacher P-J, Tastevin G. In-vivo NMR of hyperpolarized 3He in the human lung at very low magnetic fields. J Magn Reson 2003;162:122–132.
43. Eberle B, Weiler N, Markstaller K, et al. Analysis of intrapulmonary O2 concentration by MR imaging of inhaled hyperpolarised 3He. J Appl Physiol 1999;87:2043–2052.
44. de Lange EE, Altes TA, Wright CM, Mata JF, Harding DA, Harrell FE. Hyperpolarized gas MR imaging of the lung: safety assessment if inhaled helium-3. In: Proceedings of the 89th Scientific Assembly and Annual Meeting of the Radiological Society of North America. Chicago: Radiological Society of North America; 2003: 525.
45. Frahm J, Haase A, Matthaei D. Rapid NMR imaging of dynamic processes using the FLASH technique. Magn Reson Med 1986;3: 321–327.
46. Wild JM, Woodhouse N, Paley MN, Said Z, Fichele S, Kasuboski L, van Beek EJR. Comparison of 3D and 2D gradient echo for human lung ventilation with hyperpolarized 3He. In: Proceedings of the 12th Annual Meeting of ISMRM, Kyoto, Japan, 2004. (abstract 504).
47. Zhao L, Mulkern R, Tseng CH, et al. Gradient-echo imaging considerations for hyperpolarized 129Xe MR. J Magn Reson B 1996; 113:179–183.
48. Mugler III JP, Salerno M, de Lange EE, Brookeman JR. Optimized trueFISP hyperpolarized 3He MRI of the lung yields a 3-fold SNR increase compared to FLASH. In: Proceedings of the 10th Annual Meeting of ISMRM, Honolulu, 2002. (abstract 2019).
49. Kauczor HU, Ebert M, Kreitner KF, et al. Imaging of the lungs using 3He MRI: preliminary clinical experience in 18 patients with and without lung disease. J Magn Reson Imaging 1997;7:538–543.
50. Guenther D, Eberle B, Hast J, et al. 3-He MRI in healthy volunteers: preliminary correlation with smoking history and lung volumes. NMR Biomed 2000;13:182–189.
51. Mata J, Altes T, Christopher J, Mugler J, Brookeman J, de Lange E. Positional dependence of small inferior ventilation defects seen on hyperpolarized Helium-3 MR of the lung. In: Proceedings of the 9th Annual Meeting of ISMRM, Glasgow, Scotland, 2001. (abstract 949).
52. Swift AJ, Fichele S, Woodhouse N, Paley MNJ, van Beek EJR, Wild JM. Anterior to posterior variations of the ADC of inhaled 3He in healthy lungs. In: Proceeding of the 11th Annual Meeting of ISMRM, Toronto, Canada, 2003. (abstract 1402).
53. Rizi RR, Baumgardner JE, Saha PK, et al. Regional lung compliance by hyperpolarized 3Helium magnetic resonance imaging. In: Proceedings of the 9th Annual Meeting of ISMRM, Glasgow, Scotland, 2001. (abstract 944).
54. Wild JM, Fichele S, Woodhouse N, et al. Assessment and compensation of susceptibility artifacts in gradient echo MRI of hyperpolarized 3He gas. Magn Reson Med 2003;50: 417–422.
55. Woodhouse N, Swift AJ, Wild JM, Fichele S, Fleming S, Paley MNJ, van Beek EJR. Reduction of ventilated lung volumes in smokers vs non-smokers as measured by single shot fast spin echo 1H MRI and hyperpolarized 3He MRI. In: Proceedings of the 11th Annual Meeting of ISMRM, Toronto, Canada, 2003. (abstract 1399).
56. Schreiber WG, Markstaller K, Kauczor HU, et al. Ultrafast imaging of the lungs ventilation using hyperpolarized helium-3. In: Proceedings of the 7th Annual Meeting of ISMRM, Philadelphia, 1999. (abstract 2026).
57. Schreiber WG, Weiler N, Kauczor HU, et al. Ultrafast MRI of lung ventilation with hyperpolarized helium-3. Rofo Fortschr Geb Rontgenstr Neuen Bildgeb Verfahr 2000;172:129–133 [Ger].
58. Gierada DS, Saam B, Yablonskiy D, Cooper JD, Lefrak SS, Conradi MS. Dynamic echo planar MR imaging of lung ventilation with hyperpolarized ^{3}He in normal subjects and patients with severe emphysema. NMR Biomed 2000;13:176–181.
59. Mugler JP, Brookeman JR, Knight-Scott J, Maier T, de Lange EE, Bogorad PL. Interleaved echo-planar imaging of the lungs with hyperpolarized ^{3}He. In: Proceedings of the 6th Annual Meeting of ISMRM, Sydney, Australia, 1998. (abstract 448).
60. Ruppert K, Brookeman JR, Mugler JP. Real-time MR imaging of pulmonary gas-flow dynamics with hyperpolarized ^{3}He. In: Proceedings of the 6th Annual Meeting of ISMRM, Sydney, Australia, 1998. (abstract 1909).
61. Riederer SJ, Tasciyan T, Farzaneh F, Lee JN, Wright RC, Herfkens RJ. MR fluoroscopy: technical feasibility. Magn Reson Med 1998; 8:1–15.
62. Viallon M, Cofer GP, Suddarth SA, et al. Functional MR microscopy of the lung using hyperpolarized 3He. Magn Reson Med 1999;41:787–792.
63. Viallon M, Berthezene Y, Callot V, et al. Dynamic imaging of hyper-polarised (3)He distribution in rat lungs using interleaved-spiral scans. NMR Biomed 2000;13:207–213.
64. Salerno M, Altes TA, Brookeman JR, de Lange EE, Mugler JP 3rd. Dynamic spiral MR imaging of pulmonary gas flow using hyperpolarized 3He: preliminary studies in healthy and diseased lungs. Magn Reson Med 46:667–677.
65. Wild JM, Paley MNJ, Kasuboski L, et al. Dynamic radial projection MRI of inhaled hyperpolarized 3He. Magn Reson Med 2003;49: 991–997.
66. Gast KK, Puderbach MU, Rodriguez I, et al. Dynamic ventilation (3)He-magnetic resonance imaging with lung motion correction: gas flow distribution analysis. Invest Radiol 2002;37:126–134.
67. Dupuich D, Berthezene Y, Clouet PL, Stupar V, Canet E, Cremilieux Y. Dynamic ^{3}He imaging for quantification of regional lung ventilation parameters. Magn Reson Med 2003;50:777–783.
68. Tooker AC, Hong KS, McKinstry EL, Costello P, Jolesz FA, Albert MS. Distal airways in humans: dynamic hyperpolarized 3He MR imaging – feasibility. Radiology 2003;227:575–579.
69. Schreiber WG, Markstaller K, Eberle B, et al. Ultrafast MR imaging of three-dimensional distribution of hyperpolarized Helium-3 diffusion coefficient in the lung. Eur Radiol 1999;9:S542.
70. Mugler III JP, Brookeman JR, Knight-Scott J, Maier T, de Lange EE, Bogorad PL. Regional measurement of the ^{3}He diffusion coefficient in the human lung. In: Proceedings of the 6th Annual Meeting of ISMRM, Sydney, Australia, 1998. (abstract 1906).
71. Chen XJ, Möller HE, Chawla MS, et al. Spatially resolved measurements of hyperpolarized gas properties in the lung in vivo. Part I: diffusion coefficient. Magn Reson Med 1999;42:721–728.
72. Saam BT, Yablonskiy DA, Kodibagkar VD, et al. MR imaging of diffusion of ^{3}He gas in healthy and diseased lungs. Magn Reson Med 2000;44:174–179.
73. Salerno M, de Lange EE, Altes TA, Truwit JD, Brookeman JR, Mugler JP III. Emphysema: hyperpolarized helium 3 diffusion MR imaging of the lungs compared with spirometric indexes — initial experience. Radiology 2002; 222:252–260.
74. Bock M. Simultaneous T2* and diffusion measurements with ^{3}He. Magn Reson Med 1997;38:890–895.
75. Owers-Bradley JR, Fichele MS, Bennattayalah A, et al. MR tagging of human lungs using hyperpolarized ^{3}He gas. J Magn Reson Imaging 2003;17:142–146.
76. Saam B, Happer W, Middleton H. Nuclear relaxation of 3He in the presence of O_2. Phys Rev A 1995;52:862–865.
77. Deninger AJ, Eberle B, Ebert M, et al. Quantification of regional intrapulmonary oxygen partial pressure evolution during apnea by (3)He MRI. J Magn Reson 1999;141:207–216.
78. Deninger AJ, Eberle B, Bermuth J, et al. Assessment of a single-acquisition imaging sequence for oxygen-sensitive 3He-MRI. Magn Reson Med 2002;47:105–114.
79. Mata JF, Altes TA, Knake JJ, Mugler JP, Brookeman JR, de Lange EE. Hyperpolarized 3-He MR imaging of the lung: effect of subject immobilization on the occurrence of ventilation defects. In: Proceedings of the 89th Scientific Assembly and Annual Meeting, Radiological Society of North America, 2003. Chicago: Radiological Society of North America, 2003:525–526.
80. Tomiyama N, Takeuchi N, Imanaka H, et al. Mechanism of gravity-dependent atelectasis, analysis by nonradioactive xenon-enhanced dynamic computed tomography. Invest Radiol 1993;28: 633–638.

81. National Heart Lung and Blood Institute. Morbidity and mortality chartbook, 2002. http://www.nhlbi.nih.gov/resources/docs/cht-book.htm.
82. Madison JM, Irwin RS. Chronic obstructive pulmonary disease. Lancet 1998;352:467–473.
83. Swift A, Wild JM, Paley MNJ, et al. Hyperpolarized 3He MRI of normal and abnormal ventilation using a dynamic radial projection sequence. Eur Radiol 2003;13(Suppl 1):161.
84. Guenther D, Eberle B, Hast J, et al. 3-He MRI in healthy volunteers: preliminary correlation with smoking history and lung volumes. NMR Biomed 2000;13:182–189.
85. Salerno M, Mugler JP III, Cooley B, Brookeman JR, de Lange EE, Altes TA. Hyperpolarized 3He diffusion imaging in smokers: comparison with computed tomography and spirometry. In: Proceedings of the 10th Annual Meeting of ISMRM, Honolulu, 2002. (abstract 760).
86. Salerno M, Mugler JP III, de Lange EE, Brookeman JR, Altes TA. Detection of early smoking related lung disease with diffusion-weighted hyperpolarized helium-3 MR lung imaging. In: Proceedings of the 89th Scientific Assembly and Annual Meeting, Radiological Society of North America. Chicago: Radiological Society of North America; 2003:526.
87. Bhalla M, Turcios N, Aponte V, et al. Cystic fibrosis: scoring system with thin section CT. Radiology 1991;179:783–788.
88. Donnelly LF, Gelfand MJ, Brody AS, Wilmont RW. Comparison between morphologic changes seen on high-resolution CT and regional pulmonary perfusion seen on SPECT in patients with cystic fibrosis. Pediatr Radiol 1997;27:920–925.
89. Piepsz A, Wetzburger C, Spehl M. Critical evaluation of lung scintigraphy in cystic fibrosis. J Nucl Med 1980;21:909–913.
90. Donnelly LF, MacFall JR, McAdams HP, et al. Cystic fibrosis: combined hyperpolarized 3He-enhanced and conventional proton MR imaging in the lung – preliminary observation. Radiology 1999;212:885–889.
91. Altes T, Froh DK, Salerno M, et al. Hyperpolarized Helium-3 MR imaging of lung ventilation changes following airway mucus clearance treatment in cystic fibrosis. In: Proceedings of the 9th Annual Meeting of ISMRM, Glasgow, Scotland, 2001. (abstract 2003).
92. van Beek EJR, Hill C, Woodhouse N, et al. Assessment of cystic fibrosis in children using hyperpolarized 3-Helium MRI: comparison with Shwachman score, Chrispin-Norman score and spirometry. In: Proceedings of the 12th Annual Meeting of ISMRM, Kyoto, Japan, 2004. (abstract 165).
93. National Institutes of Health, National Heart, Lung, and Blood Institute. National asthma education and prevention program expert panel report 2: guidelines for the diagnosis and management of asthma. NIH Publication 97-4051. Bethesda, MD: National Institutes of Health, National Heart, Lung, and Blood Institute; 1997. 146 p.
94. Hodson ME, Simon G, Batten JC. Radiology of uncomplicated asthma. Thorax 1974;29:296–303.
95. Petheram IS, Kerr IH, Collins JV. Value of chest radiographs in severe acute asthma. Clin Radiol 1981;32:281–282.
96. Paganin F, Seneterre E, Chanez P, Daures JP, Bruel JM, Michel FB, Bousquet J. Computed tomography of the lungs in asthma: influence of disease severity and etiology. Am J Respir Crit Care Med 1996;153:110–114.
97. Newman KB, Lunch DA, Newman LS, Ellegood D, Newell J Jr. Quantitative computed tomography detects air trapping due to asthma. Chest 1994;106:105–109.
98. Altes TA, Powers PL, Knight-Scott J, et al. Hyperpolarized 3-He MR lung ventilation imaging in asthmatics: preliminary findings. J Magn Reson Imaging 2001;13:378–384.
99. de Lange EE, Altes TA, Alford BA, Mugler JP. Hyperpolarized helium-3 MR imaging of the lung in asthmatics: correlation of imaging findings with clinical symptoms and spirometry. European Society of Thoracic Imaging, Lausanne, Switzerland. Eur Radiol 2003;13:E1.
100. Samee S, Altes TA, Powers P, et al. Imaging the lungs in asthmatics using hyperpolarized helium-3 MR: assessment of response to methacholine and exercise challenge. J Allergy Clin Immunol 2003;111:1205–1211.
101. Altes T, Sara S, Ciambotti JM, Mata JF, Platts-Mills TM, de Lange EE. Hyperpolarized Helium-3 MR imaging of asthma induction. In: Proceedings of the 11th Annual Meeting of ISMRM, Toronto, Canada, 2003. (abstract 1403).
102. Lewis TA, McKinstry E, Tooker A, et al. Visualization of metacholine-induced airway constriction using hyperpolarized 3He. In: Proceedings of the 11th Annual Meeting of ISMRM, Toronto, Canada, 2003. (abstract 1406).
103. Paradis I. Bronchiolitis obliterans: pathogenesis, prevention and management. Am J Med Sci 315:161–178.
104. McAdams HP, Palmer SM, Donnelly LF, Charles HC, Tapson VF, MacFall JR. Hyperpolarized 3He-enhanced MR imaging in lung transplant patients: preliminary results. AJR Am J Roentgenol 1999;173:955–959.
105. Gast KK, Viallon M, Eberle B, et al. MRI in lung transplant recipients using hyperpolarized 3He: comparison with CT. J Magn Reson Imaging 2002;15:268–274.
106. Zaporozhan J, Gast KK, Ley S, et al. Functional analysis in single lung transplant recipients. A comparative study of high resolution CT, 3He MRI, and pulmonary function tests. Chest 2004;125:173–181.
107. Salerno M, de Lange EE, Altes TA, Brookeman JR, Jones DR, Mugler JP III. High temporal resolution interleaved-spiral dynamic hyperpolarized helium-3 MR imaging of patients with lung transplants: assessment of pulmonary gas flow as a potential method for early diagnosis of rejection. 87th Scientific Assembly and Annual Meeting, 2001, Radiological Society of North America, Chicago. Radiology 2001;221(Suppl):631–632.